

# Cooperativity in Protein Folding: From Lattice Models with Side Chains to Real Proteins

D.K.Klimov and D.Thirumalai

*Institute for Physical Science and Technology and Department of Chemistry and Biochemistry  
University of Maryland, College Park, Maryland 20742*

**Background:** Over the last few years novel folding mechanisms of globular proteins have been proposed using minimal lattice and off-lattice models. However, the factors determining the cooperativity of folding in these models and especially their explicit relation to experiments have not been fully established.

**Results:** We consider equilibrium folding transitions in lattice models with and without side chains. A dimensionless measure,  $\Omega_c$ , is introduced to quantitatively assess the degree of cooperativity in lattice models and in real proteins. We show that larger values of  $\Omega_c$  resembling that seen in proteins are obtained in lattice models with side chains (LMSC). The enhanced cooperativity in LMSC is due to the possibility of denser packing of side chains in the interior of the model polypeptide chain. We also establish that  $\Omega_c$  correlates extremely well with  $\sigma = (T_\theta - T_f)/T_\theta$ , where  $T_\theta$  and  $T_f$  are collapse and folding transition temperatures, respectively. These theoretical ideas are used to analyze folding transitions in various two state folders (RNase A, chymotrypsin inhibitor 2, fibronectin type III modules, and tendamistat) and three state folders (apomyoglobin and lysozyme). The values of  $\Omega_c$  extracted from experiments show a correlation with  $\sigma$  (suitably generalized when folding is induced by denaturants or acid). For lattice models and for proteins  $\Omega_c \sim \exp[-(\sigma/\sigma_0)^\beta]$ , where  $\beta \lesssim 1$ .

**Conclusions:** A quantitative description of cooperative transition of real proteins can be made by lattice models with side chains. The degree of cooperativity in minimal models and real proteins can be expressed in terms of the single parameter  $\sigma$ , which can be estimated from experimental data.

**Key words:** Lattice models with side chains, cooperativity of folding, collapse and folding transition temperatures, chemical and thermal unfolding.

## I. INTRODUCTION

In recent years, considerable insight into thermodynamics and kinetics of protein folding has been gained using simple lattice and off-lattice models [1–6]. The simplicity of these models allows for exhaustive sampling of the available conformational space, so that a detailed picture of the folding mechanisms can be obtained. In almost all these studies only a very coarse grained description of the polypeptide chain is retained. These models can be viewed as providing, in an approximate way, a simple representation of the  $\alpha$ -carbons of proteins. The amino acid residues are represented as single beads, which is very much in spirit of united atom approach. Mapping the characteristics of such a coarse grained description onto real polypeptide chains suggests that each bead may correspond to 2-3 amino acid residues [7,26]. Lattice models (LM) further restrict positions of the beads to the vertices of

an appropriate lattice. With the exception of the works by Skolnick and coworkers [8] most of the lattice studies have utilized simple versions of cubic and square lattices.

Despite the success of the minimal models of proteins in providing general principles of folding mechanisms there are several issues that have to be resolved before a realistic description of folding can be provided. In this article, we confine ourselves to one issue, namely, to what extent is the cooperativity of folding from an unfolded state to the native conformation mimicked by various minimal models. It is known experimentally that under optimal folding conditions proteins (especially small ones) fold in a highly cooperative manner, i.e., they exhibit an all-or-none transition [9]. This implies that there are only two relevant thermodynamic states, namely, the unfolded state ( $\mathbf{U}$ ) and the native folded conformation ( $\mathbf{N}$ ). The transition  $\mathbf{U} \rightleftharpoons \mathbf{N}$  is a first order like phase transition, implying that there is a barrier (often modest) separating the two states. The first order nature of folding transition has been seen in various minimal models of proteins for a variety of interaction schemes. Furthermore, it has been shown by various groups that this transition is a cooperative [1–6,10–13] depending on a number of factors, which are intrinsic to the sequence. However, it has not been established the degree to which this cooperativity mimics that seen in real proteins.

To address this issue quantitatively, we study lattice models with and without side chains with the purpose of assessing the extent to which cooperativity of folding transition in real protein is mimicked by these models. We introduce a dimensionless measure of cooperativity that allows us to compare theoretical models and data on real proteins on nearly equal footing. Previous studies have also addressed the factors that determine the cooperativity of folding using simplified models [8,14,15]. Hao and Scheraga showed, using a model similar to that employed here, that cooperativity of folding transitions results from proper long ranged interactions [14,15]. More recently, Skolnick and coworkers have used a high coordination lattice with each side chain having many rotamer degrees of freedom [8]. They showed that cooperativity, as measured by the sharpness of the specific heat curves, results from tight side chain packing [16,17]. These results together with our analysis using the cooperativity measure clearly show that to achieve realistic description of thermodynamics one has to include the rotamer degrees of freedom (at least approximately) into coarse grained models so that dense core packing seen in real proteins can be simulated. We establish that cooperativity can be linked to experimentally measurable quantities, namely, the collapse transition temperature  $T_\theta$  and the folding transition temperature  $T_f$ . Both  $T_\theta$  and  $T_f$  are dependent on sequence, pH, and concentration of denaturants.

## II. METHODS

### A. Lattice Model with Side Chains (LMSC)

A protein with side chains is modeled on a cubic lattice by a backbone sequence of  $N$  beads, to which a "side" bead, representing a side chain, is attached. This method of incorporating the rotamer degrees of freedom in lattice models is similar to that proposed by Bromberg and Dill [18]. In this coarse grained description, the peptide bond and the  $\alpha$ -carbon are given by a single bead. The system has in total  $2N$  beads. The following types of interactions are included in this model. (i) Self-avoidance, i.e. any backbone and side

beads cannot occupy the same lattice site more than once. (ii) The interactions between side beads  $i$  and  $j$  ( $|j - i| \geq 1$ ) are taken to be pairwise and are assumed to be given by statistical potentials derived by Kolinski, Godzik, and Skolnick (KGS) (ref. [19], Table III). We assume that, if two side beads  $i$  and  $j$  ( $|j - i| \geq 1$ ) are nearest neighbors on a lattice, they form a contact and the energy of their interaction is given by the KGS potential matrix element associated with the residues  $i$  and  $j$ . The interaction energies in the KGS interaction matrix are in units of  $kT$ , where  $T$  is the absolute temperature. In two dimensional representation we have also tried Miyazawa-Jernigan (MJ) [20,21] parameterization of the matrix of contact interactions between amino acids as well as random site interaction model.

In this study, we took  $N = 15$ . It is known that the total number of symmetry unrelated self-avoiding conformations on a cubic lattice (i.e., for a model without side chains) is 93,250,730 for  $N = 15$  [22]. Introduction of side beads dramatically increases the available conformational space, and hence exact enumeration of all conformations is no longer feasible even for  $N = 15$ . To illustrate the sharp increase in the number of available conformations we take square lattice as an example. On a square lattice the total number of symmetry unrelated conformations is 296,806 for  $N = 15$  [10]. When side beads are attached the number of available conformations becomes 653,568,850 and the corresponding number of backbone conformations is 204,988. The number of backbone conformations is reduced because many compact backbone conformations are now inaccessible due to side chain overlaps. Therefore, inclusion of side chain rotamers in the model increases the number of conformations by a factor of 2202. In the case of cubic lattice this factor would be even larger because the coordination number for cubic lattice is 6 instead of 4 for a square lattice. Thus, one has to resort to Monte Carlo methods to obtain thermodynamic characteristics of sequences even for  $N = 15$  for cubic lattice models with side chains. The maximum number of nearest neighbor contacts  $c$  in a fully compact structures also increases, when side chains are included. In our our previous work [22] we showed that for  $N = 15$   $c$  is 11 in the model without side chains. For models with side chains included this number increases to 22, when only the contacts between side chains are counted. The maximum total number of nearest neighbor contacts between backbone beads as well as side chains is 30. The larger value of  $c$  gives rise to a denser packing of the interior, and hence to a greater degree of cooperativity.

### B. Selection of Sequences and Determination of Native Structures

We generated, at random, several sequences using the constraint that the fraction of hydrophobic residues in a sequence be approximately 0.5 as in the case of naturally occurring proteins. Random sequences are most likely to be not protein-like. In order to obtain viable protein-like sequences we utilized the Z score optimization of random sequences [23–25] having unique ground states. The idea of Z score optimization is based on minimizing the relative difference between the energy of a sequence in the target conformation  $E_0$  and the average energy of misfolded structures  $E_{ms}$ , an estimate for which is  $E_{ms} = c \langle B \rangle$ , where  $c$  is number of nearest neighbor contacts in misfolded structures (presumably equal to the number of contacts in the native conformation) and  $\langle B \rangle$  is the average contact energy calculated for a particular sequence. Thus, the quantity minimized in the course of optimization procedure is

$$Z = \frac{E_0 - E_{ms}}{\delta} \quad (1)$$

where  $\delta$  is the standard deviation of contact energies for a given sequence. Standard deviation  $\delta$  and  $E_{ms}$  are sequence dependent quantities. Low values of  $Z$  would correspond to sequences with large stability gaps ( $E_{ms} - E_0$ ) [2] and small  $\delta$ . The sequence with lowest  $Z$  score for a given sequence composition is found by performing Monte Carlo simulations in sequence space, the details of which are given elsewhere [22,24,25]. In this study, we used simulated annealing protocol when doing Monte Carlo simulations in sequence space and we produced a total of 20 trajectories. In the course of simulations we constantly monitored  $Z$  score values and in the end selected sequences with low values of  $Z$ .

Target conformations used in optimization procedure were randomly chosen from preliminary Monte Carlo simulations subject to the conditions that these structures be reasonably compact, and have a unique contact map (in order to avoid degeneracy of a ground state). When a sequence was optimized, we verified that the target conformation indeed corresponds to the lowest energy state. To this end, we generated 20 slow cooling Monte Carlo trajectories starting with different initial conditions at high enough temperature, at which sequences are in random coil conformations. The final temperature of these simulations is set to 0.05, which is well below the folding transition temperature,  $T_f$ . We were unable to find any conformation, which has lower energy for selected sequence than the target structure. We also constantly monitored energies in all the dynamic simulations. In no instance did we find energies lower than that corresponding to the native state. The energies and temperature in this study are expressed in the units of  $kT$  and  $T$ , respectively, where  $T$  is an absolute temperature.

### C. Probes of Thermodynamics of Sequences: Computation of $T_\theta$ and $T_f$

Thermodynamics of a given sequence was probed using the overlap function  $\chi$  [10,22] and its fluctuation  $\Delta\chi$  suitably modified for the lattice model with side chains. The overlap function, which describes the overall conformation of a sequence in relation to the native state  $\mathbf{N}$  is defined as

$$\chi = 1 - \frac{1}{2N^2 - 3N + 1} \left( \sum_{i < j} \delta(r_{ij}^{ss} - r_{ij}^{ss,N}) + \sum_{i < j+1} \delta(r_{ij}^{bb} - r_{ij}^{bb,N}) + \sum_{i \neq j} \delta(r_{ij}^{bs} - r_{ij}^{bs,N}) \right), \quad (2)$$

where  $r_{ij}^{bb}, r_{ij}^{ss}, r_{ij}^{bs}$  refer to the distances between backbone beads, between side beads, and between backbone and side beads, respectively. The factor  $2N^2 - 3N + 1$  ensures that in the native conformation  $\chi = 0$ . We also studied the partitioned overlap functions,  $\chi_{ss}$  and  $\chi_{bb}$ , which are defined by

$$\chi_{ss} = 1 - \frac{2}{N^2 - N} \sum_{i < j} \delta(r_{ij}^{ss} - r_{ij}^{ss,N}) \quad (3)$$

and

$$\chi_{bb} = 1 - \frac{2}{N^2 - 3N + 2} \sum_{i < j+1} \delta(r_{ij}^{bb} - r_{ij}^{bb,N}). \quad (4)$$

The backbone overlap  $\chi_{bb}$  measures the content of a native backbone, while the side chain overlap  $\chi_{ss}$  measures the "nativeness" of side chain conformations. By treating these quantities separately it is easier to monitor the onset of native character in the backbone and side chains.

The acquisition of the overall native state (backbone plus side chains) was also probed using the probability of being in the native structure (a single microstate)

$$P_0 = \frac{\sum_i \delta(\chi_i) e^{-\frac{E_i}{T}}}{\sum_i e^{-\frac{E_i}{T}}}. \quad (5)$$

In order to observe the acquisition of the native conformation of the backbone and side beads separately, we have calculated the probability that the backbone is in the native structure

$$P_0^b = \frac{\sum_i \delta(\chi_{i,bb}) e^{-\frac{E_i}{T}}}{\sum_i e^{-\frac{E_i}{T}}} \quad (6)$$

and, similarly, the probability of side chains to be in the native positions

$$P_0^s = \frac{\sum_i \delta(\chi_{i,ss}) e^{-\frac{E_i}{T}}}{\sum_i e^{-\frac{E_i}{T}}}. \quad (7)$$

It may seem that there is no need to consider  $P_0^s$  separately from  $P_0$ , because there are not many ways of changing the backbone conformation while keeping the side chain contacts intact. Indeed, analysis shows that there are very few conformations, which do allow such changes, but they constitute a small fraction of all structures so their contribution would be negligible. Our simulations show that unless these structures have a considerable Boltzmann weight (that is highly unlikely) there is no appreciable difference between  $P_0$  and  $P_0^s$ .

In Eqs. (5,6,7) the various probabilities correspond to one microstate associated with the native conformation, which is an artifact of lattice models. This is physically unrealistic because in any realistic description there is a volume associated with the native basin of attraction (NBA). Thus, many conformations will map onto the NBA. It is, therefore, more relevant to calculate the probability of being in the NBA

$$P_{NBA} = \frac{\sum_i \delta(\chi_i \leq \chi_{NBA}) e^{-\frac{E_i}{T}}}{\sum_i e^{-\frac{E_i}{T}}}. \quad (8)$$

In Eq. (8) the sum is taken over all possible conformations of backbone and side chains, and  $\chi_{NBA}$  is the value of overlap at the temperature, when the fluctuations of  $\chi$  are maximum, i.e.  $\chi_{NBA} = \langle \chi(T_f) \rangle$  (see below). At and below  $T_f$  conformations with  $\chi \leq \chi_{NBA}$  will map onto the NBA. It is clear that  $P_{NBA}$  is physically more relevant than  $P_0$ . This is because thermal fluctuations in real proteins frequently sample numerous conformations proximal to the native conformation.

In addition to the functions described above, we calculated the energy  $\langle E \rangle$ , the specific heat  $C_v$ , and the radius of gyration  $R_g$  using standard definitions. The collapse transition temperature  $T_\theta$  was determined from the maximum of specific heat  $C_v$  [10,22,26] and was found to be well correlated with the temperature, at which the rate of change of the radius of gyration  $R_g$  becomes maximum. As before the folding transition temperature  $T_f$  was inferred from the peak of the overlap fluctuation  $\Delta\chi$  [10,22,26].

#### D. Calculation of thermodynamic quantities

The thermodynamic quantities were computed using the multiple histogram technique [27], which has been implemented in the following way. From the slow cooling simulations used to determine the native conformations a rough estimate of collapse and folding transition temperatures,  $T_\theta$  and  $T_f$ , can be made. This allows us to select the temperature range, in which histograms are to be collected. At each temperature histograms were collected using  $M = 100 - 200$  Monte Carlo trajectories, each with different initial conditions. Each trajectory starts at high temperature  $T_h \gtrsim T_\theta$  and ends at the temperature  $T_l \simeq T_f$ . In the course of a trajectory the temperature is changed every  $t$  Monte Carlo steps (MCS) according to the schedule  $T_r = T_h - r\Delta T$ , where  $r = 0, \dots, (T_h - T_l)/\Delta T$  and the typical value of  $\Delta T$  is 0.05. Accordingly, histograms were collected at the temperatures  $T_r$  using  $M$  trajectories generated. In total, we have  $R = (T_h - T_l)/\Delta T + 1$  histograms. Five variables were used to collect histograms, these are overlap function  $\chi$ , backbone overlap  $\chi_{bb}$ , side chain overlap  $\chi_{ss}$ , energy  $E$ , and the square of the radius of gyration  $R_g^2$ . The length of the trajectory at fixed temperature  $T_r$  was set constant for all temperatures and sequences at the value of  $t = 2 \times 10^7$  MCS. It is important to note that a portion of trajectory immediately following temperature change must be excluded in order to allow the chain to equilibrate at a new  $T$ . We found this interval of equilibration does not exceed  $2 \times 10^6$  MCS at the lowest temperature for all sequences. For simplicity, the equilibration interval was kept constant for all temperatures. While collecting states in the histograms we used 0.1 grid intervals for the energy  $E$  and the square of the radius of gyration  $R_g^2$  and exact discrete values for functions  $\chi$ ,  $\chi_{bb}$ , and  $\chi_{ss}$ .

The thermodynamic average of a quantity  $A$  that is a function of, say,  $\chi$  and  $E$  is calculated using multiple histogram method as follows

$$A = \frac{\sum_E \sum_\chi A(E, \chi) e^{-\frac{E}{T}} \frac{\sum_{r=1}^R h(E, \chi)(T_r)}{\sum_{r=1}^R n_r e^{f_r - \frac{E}{T_r}}}}{\sum_E \sum_\chi e^{-\frac{E}{T}} \frac{\sum_{r=1}^R h(E, \chi)(T_r)}{\sum_{r=1}^R n_r e^{f_r - \frac{E}{T_r}}}} \quad (9)$$

where  $R$  is the number of histograms,  $T_r$  is the temperature of simulations, at which  $r$ th histogram is collected,  $n_r$  is the number of states in the  $r$ th histogram, and  $f_r$  is the scaled free energy to be calculated self-consistently from the following equation

$$e^{-f_r} = \sum_E \sum_\chi e^{-\frac{E}{T_r}} \frac{\sum_{m=1}^R h(E, \chi)(T_m)}{\sum_{m=1}^R n_m e^{f_m - \frac{E}{T_m}}} \quad (10)$$

The values of  $f_r$  can be determined from an iterative scheme within less than 300 iterations with excellent accuracy.

Using the multiple histogram technique we have calculated overlap function  $\langle \chi \rangle$ , its fluctuation  $\Delta\chi$ , backbone overlap  $\langle \chi_{bb} \rangle$ , its fluctuation  $\Delta\chi_{bb}$ , side chain overlap  $\langle \chi_{ss} \rangle$ , its fluctuation  $\Delta\chi_{ss}$ , energy  $\langle E \rangle$ , specific heat  $C_v$ , probabilities of occupancy of the native state  $P_0$ ,  $P_0^b$ ,  $P_0^s$  and the NBA  $P_{NBA}$ , and the radius of gyration  $\langle R_g \rangle$  as functions of temperature. From these the key characteristic temperatures  $T_\theta$  and  $T_f$  can be readily computed.

### III. RESULTS AND DISCUSSION

#### A. Thermodynamics of sequence A and B

For the present study we have considered three sequences in three dimensional (3D) LMSC each with a unique ground state. In order to keep the description compact we describe in detail the thermodynamics associated with two sequences, A and B. The general characteristics of the third sequence C are similar to those of B. The compositions of the two sequences along with their native states and energy spectra are given in Fig. (1).

In Fig. (2) temperature dependencies of various thermodynamic functions are plotted for sequence A. The collapse transition temperature  $T_\theta$  is determined from the peak of  $C_v$  (see Fig. (2c)) and is equal to 0.27. As shown in Fig. (2c) this temperature coincides with the temperature, at which the derivative  $d \langle R_g \rangle / dT$  shows maximum. This is a strong evidence that  $T_\theta$  indeed corresponds to the temperature, at which the transition from a random coil state to an ensemble of compact structures takes place. The plot of  $\langle \chi \rangle$  (measuring the content of native state) shows that equilibrium refolding occurs highly cooperatively, indicating a two state transition. Note that the plot of  $\langle \chi_{bb} \rangle$  follows  $\langle \chi \rangle$  very closely. It can be seen in Fig. (2b) that the fluctuations in the functions  $\chi$  and  $\chi_{bb}$  (as well as  $\chi_{ss}$ , not shown) display a well defined peak at the temperature  $T_f = 0.26$ . This value coincides with the temperature, at which the probability of being in the NBA is 0.5 (see Fig. (2d)). Thus, evaluations of  $T_f$  from  $\Delta\chi$  and  $P_{NBA}$  are equivalent. It is seen that the backbone fluctuations  $\Delta\chi_{bb}$  are stronger at  $T_f$  than the fluctuations of the entire sequence. Thus, for sequence A the value of parameter  $\sigma_T$  is 0.04 (see below).

It is of interest to compare the probabilities  $P_0$  and  $P_0^b$  as a function of temperature. We find that the native backbone is formed prior to the formation of the entire native conformation as the temperature is lowered (data not shown). In fact, the native backbone is predominantly populated at  $T \leq T_0^b = 0.22$ , whereas the complete native structure becomes overwhelmingly populated only at  $T \lesssim 0.17$ . This observation suggests that as the temperature decreases backbone conformation becomes frozen, while side chains still have no well defined conformations seen in the native structure.

Our analysis indicates that sequence A is a two-state folder. This is readily inferred from Figs. (2a) and (2b). This point is further illustrated by plotting the thermally weighted distribution of  $(\chi, E)$  states at  $T \simeq T_f$ . Such plots can be readily obtained from multiple histogram calculations. In Fig. (3) we plot the two dimensional histogram of  $(\chi, E)$  states for sequence A (upper panel). The main feature of this plot is that it clearly reflects the localization of sequence in two distinctive states shown in red with very different values of overlaps and energies - folded (NBA) and unfolded states. Kinetic simulations (D.K. and D.T., unpublished) suggest that the second (unfolded) state consists of open random coil conformations. Therefore, we classify sequence A as a two state folder.

The thermodynamic analysis for sequence B gives  $T_\theta = 0.44$ . At roughly the same temperature ( $=0.48$ )  $d \langle R_g \rangle / dT$  has a maximum indicating that  $T_\theta$  does correspond to the collapse transition. The value of  $T_f = 0.30$  and hence  $\sigma = 0.32$ . Due to this relatively large  $\sigma$  value we expect the folding transition to be better described by a multistate behavior. This is in fact the case and can be seen most clearly from the two dimensional histogram of  $(\chi, E)$  states displayed in the lower panel of Fig. (3). This plot for sequence B shows that,

at the folding transition temperature, the model polypeptide chain samples at least three distinctive thermodynamic states shown in red with  $\chi \simeq 0.0$ ,  $\chi \simeq 0.3$ , and  $\chi \simeq 0.65$ . Notice that the energies at these values of  $\chi$  are also different. Based on this analysis we expect the folding of B to be less cooperative than A.

### B. Comparing cooperativity for LMSC and LM

The structures of the native states and the corresponding low energy spectra for the two sequences A and B are given in Fig. (1). Even though the chain length is small it is seen that an interior of the native state of a sequence A is more tightly packed than that of B. By contrast, sequence B has less well formed interior and hence has a lesser degree of side chain packing. Specifically, the radius of gyration of a hydrophobic core  $R_{g,H-H}$  (which measures the average distance between hydrophobic residues) calculated for the native structure of sequence A is equal to 1.2. In contrast,  $R_{g,H-H}$  obtained for sequence B is found to be 1.25. It is also interesting to point out that the average distance between hydrophilic residues in the native structure of sequence A is considerably larger (equal to 2.3) when compared with that found for sequence B (equal to 1.9). This suggests that the core of sequence A has significant hydrophobic clustering that leads to denser packing than in sequence B. The low energy spectra of these sequences also reveal different behavior. The first excited state of sequence A has the backbone in a non-native conformation, while the first few excited states of B all have the native conformation for the backbone. The energy gap (the difference between the native state and the first excited state) and the so called stability gap [2] (the energy difference between the native conformation and misfolded structures) are larger for sequence B than for sequence A. Nevertheless, it is shown below that sequence A folds more cooperatively than sequence B indicating that the gaps (however they are defined) are by themselves not a good indicator of cooperativity.

In order to compare the degree of cooperativity in various models and real proteins we introduce the dimensionless cooperativity index defined as

$$\Omega_c = T_{max}^2 \frac{\max[\frac{d\langle\chi\rangle}{dT}]}{\Delta T}, \quad (11)$$

where  $\Delta T$  is the full width at the halfmaximum of the peak of  $d\langle\chi\rangle/dT$  and  $T_{max}$  is the temperature, at which  $d\langle\chi\rangle/dT$  has a peak. This quantity can be calculated for other measures such as the temperature or denaturant dependence of the fraction of native state, which are experimentally measurable.

There are other measures of cooperativity that could be used. One such criterion is based on the van't Hoff equation, from which an index of cooperativity, namely,  $\Omega_{VH} = \Delta H \Delta T / RT_{max}^2$  may be introduced. For an infinitely sharp two-state transition  $\Omega_{VH} \rightarrow const$ , while for a completely non-cooperative transition  $\Omega_{VH} \rightarrow 0$ . Our criterion, on the other hand, gives  $\Omega_c \rightarrow \infty$  for an infinitely sharp two-state transition and tends to zero, when the transition is non-cooperative. This provides a wider spread in  $\Omega_c$  and we expect it to lead to easier calibration of cooperativity. Furthermore, when only the dependence of order parameter (like fraction of native state) as a function of denaturant concentration is available, a suitable generalization of Eq. (11) can be readily used to compute  $\Omega_c$ , whereas the generalization of  $\Omega_{VH}$  to this case is not obvious.



We have shown elsewhere [10,22,26,28] that folding kinetics (i.e., the time required to reach the native conformation) is well correlated with

$$\sigma_T = \frac{T_\theta - T_f}{T_\theta}, \quad (12)$$

i.e., sequences with small  $\sigma$  reach the native state more rapidly than those with larger  $\sigma$ . Folding is most rapid near the tricritical point ( $T_f \approx T_\theta$ ), at which collapse and acquisition of the native state are almost synchronous. Parenthetically, we note that other criteria for identifying fast folding sequences have been proposed [2,6].

The value of  $\Omega_c$  for sequence A is 5.32, for sequence B it is 2.03, and for the third sequence, C,  $\Omega_c = 1.80$ . Comparing  $\Omega_c$  for sequences A, B, and C shows that *cooperativity is also determined by  $\sigma$* ;  $\sigma$  for A is 0.04, for B is 0.32, and for C is 0.34. This is shown (see below) to be the case for both LMSC and LM.

It is interesting to compare  $\Omega_c$  for lattice models with side chains and lattice models without side chains. For this, we consider a number of 15-mer sequences without side chains on a cubic lattice. The sequences used for this purpose are the ones studied in our previous papers [22,28]. Many of these sequences fold cooperatively with  $\sigma$  values ranging from 0.0 to 0.79. In Fig. (4) we plot  $\Omega_c$  as a function of  $\sigma$  for 15-mer lattice sequences. The maximum value of  $\Omega_c$  of 3.0 is observed for sequences with  $\sigma \simeq 0.0$ . This level of cooperativity is less than that seen in the models with side chains indicating that cooperativity in natural proteins results from the dense packing of side chains in the core [8,16]. Fig. (4) shows remarkable statistical correlation between the cooperativity index  $\Omega_c$  and  $\sigma$ . When combined with our previous results we can conclude that both cooperativity and folding kinetics is determined by the intrinsic thermodynamic parameters  $T_\theta$  and  $T_f$ . It should be emphasized that  $T_\theta$  and  $T_f$  are sensitive to mutations as well as external conditions such as pH, ionic strength, etc.

In order to further establish the correlation between  $\Omega_c$  and  $\sigma$  we have studied two dimensional (2D) LMSC using a number of sequences with very different interaction potentials (see caption to Fig. (5)). Sequence properties have been inferred by exhaustive enumeration of all allowed conformations. This permits us to analyze much larger sequence database than for 3D LMSC. In Fig. (5) we plot  $\Omega_c$  as a function of  $\sigma$  for our 2D models with side chains. As is the case for  $N = 15$  3D LM the correlation is excellent. It should be noted that  $\Omega_c$  values are considerably smaller than in 3D indicating that for realistic depiction of cooperativity 2D simulations may not be reliable.

### C. Dependence of $\Omega_c$ on chain length

The model with side chains for  $N = 15$  yields  $\Omega_c$  values of the order of 5, when  $\sigma$  is small, whereas real proteins, which are two state folders, have  $\Omega_c$  in excess of 10 (see below). This discrepancy between LMSC and experiments is due probably to the small value of  $N$ . If  $N$  is increased, then we expect to obtain  $\Omega_c$  in the experimentally measured range. This assertion is borne out by examining  $\Omega_c$  for lattice models without side chains for larger  $N$ . In Fig. (6) we display  $\Omega_c$  vs  $\sigma$  for 27-mer sequences, for which detailed account of thermodynamics and kinetics was provided in a previous study [22]. For  $N = 27$  we see that  $\Omega_c$  ranges from 1.0 ( $\sigma = 0.35$ ) to 33.3 ( $\sigma = 0.0$ ). This figure also shows that cooperativity is essentially determined by  $\sigma$ . The results in Figs. (4-6) show that one can write

$$\Omega_c \sim \exp[-(\sigma/\sigma_0)^\beta], \quad (13)$$

where  $\sigma_0$  is a model dependent constant and  $\beta \lesssim 1$ . Since the addition of side chains enhance  $\Omega_c$ , we conclude that in order to provide a realistic description of cooperativity in protein folding it is necessary to include side chains in minimal models of proteins.

#### D. Extracting $\Omega_c$ and $\sigma$ from experiments

We have computed  $\Omega_c$  for a few proteins and a protein fragment using experimental data such as the dependence of fraction of native state as a function of temperature, denaturant or acid [29–35]. The proteins we chose for our analysis are for illustrative purposes only and does not constitute an exhaustive analysis. The data from the literature when used in combination with Eq. (11) gives  $\Omega_c$  in the range 0.25 - 99.4 (see Tables I-III). Out of the eight proteins considered here the fragment of barnase is least cooperative [33]. This, in fact, suggests that the cooperativity is greatly compromised in the absence of long range interactions with the rest of the protein. Surprisingly, the cooperativity of the ninth module of fibronectin exhibits the level of cooperativity similar to the barnase fragment. Chymotrypsin inhibitor 2 (CI2), RNase A, tendamistat, and the tenth module of fibronectin ( $^{10}\text{FNIII}$ ) have been recently shown [29–32] to fold in a very cooperative two state manner. Apomyoglobin (apoMb) and lysozyme [34,35] have been shown to be three state folders. Below we describe the cooperativity of these proteins using the equilibrium folding data.

**Two state folders:** The thermal unfolding of RNase A and RNase B has been recently reported [30]. The data for the fraction of native state as a function of temperature (see Fig. (5) of [30]) clearly exhibits a cooperative two state transition. Using the parameters obtained from the two state analysis of RNase A in [30] and Eq. (11) (where  $\langle \chi \rangle$  is replaced by the native fraction  $f_N$ ) we get  $\Omega_c \approx 99.4$ . The large value of  $\Omega_c$  makes us suggest that for this protein  $\sigma \approx 0.0$  implying that  $T_f \approx T_\theta$ . A more precise estimate of  $\sigma$  is given below.

Kiefhaber and coworkers [31] have argued using the ellipticity measurements at pH=7 and  $T = 25^\circ\text{C}$  that tendamistat (a small protein consisting of 74 amino acid residues) unfolds thermodynamically in an all-or-none fashion upon increasing the concentration of guanidinium chloride. The value of  $\Omega_c$  calculated using the dependence of the fraction of native state  $f_N$  (see Eq.(14)) on the concentration of GdnHCl is 13.7, which is considerably less than for RNase A. This suggests that either  $\sigma$  for tendamistat is larger than for RNase A or that  $\Omega_c$  is intrinsically smaller when folding is induced by varying the concentration of denaturants as opposed to thermal unfolding. The determination of  $\sigma$  (see below) suggests that the latter is a more likely possibility.

Recently, Dobson and coworkers have shown that denaturation induced unfolding of fibronectin type III  $^9\text{FNIII}$  and  $^{10}\text{FNIII}$  proteins is well described by a two state model [32]. However, it was found that  $^9\text{FNIII}$  has a lower stability (as measured by a free energy difference between **U** and **N**) than  $^{10}\text{FNIII}$ . The free energy of unfolding in water  $\Delta G_{H_2O} = 1.2$  and  $6.1 \text{ kcal mol}^{-1}$  for  $^9\text{FNIII}$  and  $^{10}\text{FNIII}$ , respectively. In line with these observations, our analysis suggests that both proteins display sharply different degrees of cooperativity with  $\Omega_c = 0.28$  obtained for  $^9\text{FNIII}$  and 7.5 for  $^{10}\text{FNIII}$ . Accordingly, we expect that the  $\sigma$  values are very different for  $^9\text{FNIII}$  and  $^{10}\text{FNIII}$ .

A few years ago Jackson and First [29] reported that folding of CI2 proceeds via a two state manner. This was the case whether denaturation was induced chemically or thermally. By using fluorescence,  $F$ , as a function of  $[GdnHCl]$  they extracted parameters for the two-state description of the data. Since the values of  $F_N$  and  $F_U$  (fluorescence in the native state and denaturated state, respectively) were not reported we determine the fraction of native state for chemically induced unfolding using

$$f_N = \frac{F - F_N}{F_U - F_N} = \frac{1}{1 + \exp^{-\frac{\Delta G_U}{RT}}}, \quad (14)$$

where  $\Delta G_U = \Delta G_{H_2O} - m[GdnHCl]$  and  $\Delta G_{H_2O}$  is the free energy of unfolding in water,  $m$  is a constant that effectively measures the degree of exposure of the protein upon denaturation, and  $R$  is the gas constant. For Eq. (14), which gives a two-state description of denaturant induced unfolding,  $\Omega_c$  can be shown to be

$$\Omega_c = \frac{1}{4} \left( \frac{\Delta G_{H_2O}}{RT} \right)^2 \frac{1}{\ln \frac{3+2\sqrt{2}}{3-2\sqrt{2}}}, \quad (15)$$

implying that cooperativity in this case is directly related to stability [37]. Using the experimental parameters  $\Delta G_{H_2O} = 7.03 \text{ kcal mol}^{-1}$  and  $m = 1.79 \text{ kcal mol}^{-1} M^{-1}$  [29] we find  $\Omega_c = 9.9$  - a value that is comparable to tendamistat.

Jackson and Fersht also reported thermally induced unfolding of CI2 as a function of pH [29]. They measured the pH dependence of the folding transition temperature  $T_f$  (referred to as  $T_m$  in ref. [29]) using scanning microcalorimetry experiments. They showed that in the range of pH (2.2-3.5) CI2 unfolds thermally also by a two state manner. We calculated  $\Omega_c$  using the data given in [29] and find that it lies between 5.9 at pH=2.2 to 29.3 at pH=3.5. The degree of cooperativity clearly increases with pH. At the higher values of pH  $\Omega_c$  is larger than that found by chemical denaturation. Thus, in general, it appears that the degree of cooperativity is greater when unfolding is induced thermally than by adding denaturants.

We have established in the simulations on lattice models that  $\Omega_c$  is well correlated with  $\sigma_T$  (see Figs. (4-6)). In order to verify this in experiments one needs measurements of  $T_\theta$ , which are not currently available. So we have devised a way to obtain  $T_\theta$  using the following arguments. Since there are two separate phase transitions at  $T_\theta$  and  $T_f$  the experimental determination of  $\sigma$  requires separate measurements of order parameters, probing these "phases". The estimate of  $T_\theta$  requires independent measurement of a quantity associated with the compaction of a polypeptide chain (for example, the radius of gyration,  $R_g$ ). At present, simultaneous measurements of  $R_g$  and the fraction of native state  $f_N$  are extremely rare [35]. In the absence of such measurements we have used an ad hoc empirical procedure to estimate  $\sigma$  from the existing data so that the variation of  $\Omega_c$  with pH, such as that seen in CI2, can be rationalized. To estimate  $T_\theta$  from experiments we propose the following approach. We calculated  $T'_\theta$  (an estimate for  $T_\theta$ ) using the condition

$$f_N(T'_\theta) = C, \quad (16)$$

where  $C$  here is taken to be 0.05. At  $T_\theta$  the equilibrium is shifted almost to the unfolded state and, consequently, we expect  $C$  in Eq. (16) to be small. Recall that  $T_f$  is determined in the analysis of experimental data from  $f_N(T_f) = 0.5$ .

In order to justify the use of Eq. (16) we have estimated  $T'_\theta$  using  $P_0(T'_\theta) = 0.05$  for LM with  $N = 27$ . A plot of  $T'_\theta$  from this estimate as a function of actual  $T_\theta$  (from the peak of the specific heat) is given in Fig. (7). There is a very good correlation (with the slope being near unity) with the quality getting better as  $T_\theta$  becomes larger, which corresponds to small  $\sigma$  values. A similar correlation is found when  $C$  is changed to 0.1. This method of estimating  $T_\theta$ , although arbitrary, is physically motivated. We find that if  $C$  is increased beyond 0.1 the correlation coefficient considerably decreases. Thus, this way of obtaining  $T_\theta$  from experimental data (with  $C \lesssim 0.1$ ) is useful especially for the two state folders.

Additional justification of the use of Eq. (16) to estimate  $T_\theta$  can be given by examining the temperature dependence of  $R_g$  for RNase A. Sosnick and Trewhella have used small X-ray scattering to measure  $R_g$  as a function of temperature (see Fig. (2) of [36]). For the nonreducing conditions, which were the ones considered in [30] as well, we estimate  $T_\theta$  (from Fig. (2) in [36]) to be around 66°C. This value is remarkably close to that obtained using Eq. (16) ( $T_\theta \simeq 65.2^\circ\text{C}$ ) using the data of Ulbrich-Hofmann and coworkers. We should emphasize that despite the reasonable estimates of  $T_\theta$  from Eq. (16) independent experimental measurements are needed.

We have used Eq. (16) together with the data on thermal unfolding of CI2 and RNase A to estimate  $T_\theta$ . These are given in Table I along with their  $\Omega_c$  and  $\sigma$ . It is seen from Table I that  $\sigma_T$  is relatively large for CI2 at pH=2.2. From the previously established results connecting folding kinetics and  $\sigma$  [22,28,26] we predict that there should be a significant off-pathway process in the refolding of CI2 at pH=2.2 at  $T \approx T_f$ . It would be interesting to determine the pH dependence (over a wider range) of  $T_f$  for the variant of CI2 used in the recent experiments of Fersht and coworkers, which contains 64 amino acid residues as opposed to 81 in the original work of Jackson and Fersht.

In most of the experiments the equilibrium unfolding is achieved by chemical denaturation. The analysis of such experiments can be done by generalizing  $\sigma$ . We introduce

$$\sigma_D = \frac{C_\theta - C_f}{C_\theta}, \quad (17)$$

where  $C_\theta$  is the concentration of denaturant, at which the transition to compact structures from the random coil state takes place, and  $C_f$  is the denaturant concentration in the midpoint of an appropriate measure of the native state population. Similarly,  $\Omega_c$  in Eq. (11) can be calculated using the denaturant dependence of the fraction of native state. With this generalization we have estimated  $C_f$  and  $C_\theta$  for tendamistat, <sup>9</sup>FNIIL, <sup>10</sup>FNIIL, and CI2 (denaturant induced unfolding). The value of  $C_\theta$  is obtained from the condition  $f_N(C_\theta) = 0.05$ . The values of  $\sigma$  and  $\Omega_c$  are given in Table II.

The physical basis for proposing Eq. (17) as a natural generalization of Eq. (12) is the following. When the temperature changes from below  $T_f$  to above  $T_\theta$ , there are two phase changes, one at  $T_f$  and the other at  $T_\theta$ . Similar phase changes are seen upon chemical denaturation. Both  $\sigma_D$  and  $\sigma_T$  capture the physics that fastest folding should occur when the intermediate is eliminated. Quantitatively, the value of  $\sigma_D$  and  $\sigma_T$  need not coincide because the nature of interactions due to thermal unfolding and denaturant induced unfolding is different. In fact, it appears from the analysis of the experiments in this study that thermal denaturation is sharper than chemically induced unfolding.

**Three State Folders:** Barrick and Baldwin [34] showed that urea and acid induced folding

of apomyoglobin (apoMb) is best described by a three state model. Thus, the equilibrium folding is given by



Here we analyze the acid induced transition using the data presented in Fig. (1) and Table I of [34]. In Fig. (1) of [34] Barrick and Baldwin present the helical content of apoMb as a function of pH at various urea concentrations. We have ignored the data at 4.5 M concentration of urea, because there appears to be no significant change in  $[\theta]_{222}$  with pH as measured by CD spectroscopy. At 3.0 M the value of  $[\theta]_{222}$  at the highest pH is considerably less than at all other values of urea concentration, which does not seem to be reflected in the quantitative analysis presented in Table I of [34]. Examination of all other curves clearly shows evidence for three state behavior. If we calculate  $\Omega_c$  for the transition  $\mathbf{U} \rightleftharpoons \mathbf{N}$ , ignoring the equilibrium intermediate  $\mathbf{I}$ , we find that the overall cooperativity is highly compromised. For the purposes of measuring the cooperativity of folding we have focused separately on the transitions  $\mathbf{U} \rightleftharpoons \mathbf{I}$  and  $\mathbf{I} \rightleftharpoons \mathbf{N}$  and calculated  $\Omega_c(\mathbf{U} \rightleftharpoons \mathbf{I})$  and  $\Omega_c(\mathbf{I} \rightleftharpoons \mathbf{N})$  using a simple generalization of Eq. (12). An estimate of  $\sigma_{pH}$  can be easily made by associating the midpoint of the transition  $\mathbf{U} \rightleftharpoons \mathbf{I}$  with the collapse process and the midpoint of the transition  $\mathbf{I} \rightleftharpoons \mathbf{N}$  with the folding transition. The values of  $\Omega_c$  and  $\sigma_{pH}$  for acid induced refolding are given in Table III. It is clear that  $\Omega_c$  is largest for the smallest values of  $\sigma_{pH}$ , which is consistent with the results for LMSC and LM and the two state folders. In Table III we also present the cooperativity index  $\Omega_c(\mathbf{U} \rightleftharpoons \mathbf{I})$  for apoMb. It is clear from Table III that  $\Omega_c(\mathbf{U} \rightleftharpoons \mathbf{I})$  is considerably less than  $\Omega_c(\mathbf{I} \rightleftharpoons \mathbf{N})$  at all values of urea concentration. The very small values of  $\Omega_c(\mathbf{U} \rightleftharpoons \mathbf{I})$  suggest that the initial compaction results in the formation of an equilibrium intermediate, whose structural characteristics are closer to  $\mathbf{U}$  than to  $\mathbf{N}$ .

Further evidence for our assertion that  $\mathbf{U} \rightleftharpoons \mathbf{I}$  transition in apoMb is less cooperative (as measured by  $\Omega_c$ ) comes from the recent work of Luo *et al.* [37]. These authors measured the unfolding thermodynamics from the pH 4 folding intermediate of apoMb, in which A, G, and H helices are ordered. By using mutations in the A and G helices Luo *et al.* argue that the unfolding from  $\mathbf{I}$  is well described by a two state thermodynamics. Although the authors did not explicitly provide  $\Delta G_{H_2O}$  values (needed in Eq. (14)) we scanned the data in Fig. (3) of [37] and calculated  $\Omega_c$  values. The resulting  $\Omega_c$  values for  $\mathbf{U} \rightleftharpoons \mathbf{I}$  transition is given in Table III. We find that these values are remarkably consistent with those obtained from the pH induced unfolding transition  $\mathbf{U} \rightleftharpoons \mathbf{I}$  reported in [34]. Thus, it appears that the assembly of the native state from the equilibrium intermediate  $\mathbf{I}$  is more cooperative than the formation of  $\mathbf{I}$  itself from the unfolded state.

Doniach and coworkers have argued using radius of gyration data that folding of lysozyme at pH=2.9 is better described by a three state analysis rather than by an all-or-none transition [35]. We have used the theoretical methods developed here to compute  $\sigma_D$  and  $\Omega_c$ . These are displayed in Table III. The value of  $\sigma_D$  is smaller than for apoMb. Unlike the results for apoMb the data for denaturant induced unfolding of lysozyme does not exhibit a clear evidence of a third equilibrium intermediate at pH=2.9. This observation together with relatively small value of  $\sigma$  makes us suggest that at pH=2.9 lysozyme is, at best, a borderline three state folder.

In Fig. (8) we plot  $\Omega_c$  as a function of  $\sigma$  using the data given in Tables I, II, and III. This figure shows a good correlation between two quantities. If the transition is strictly an

all-or-none, then from a mathematical representation of the resulting sigmoid curve one can show that the correlation between  $\Omega_c$  and  $\sigma$  should follow independent of the value of  $C$  used in Eq. (16) to get  $T_\theta$  (and hence  $\sigma$ ). Thus, the good correlation between  $\Omega_c$  and  $\sigma$  for two state folders is not surprising. Fig. (8) also shows a good correlation for acid induced unfolding of apoMb, which is a three state folder (see Table III). For this protein,  $T_\theta$  and  $T_f$  are calculated from the midpoints of  $\mathbf{U} \rightleftharpoons \mathbf{I}$  and  $\mathbf{I} \rightleftharpoons \mathbf{N}$  transitions, respectively. Thus, we feel that the degree of cooperativity in protein folding can be understood in terms of  $\sigma$  with  $T_\theta$  being empirically defined by Eq. (16). The physically motivated choice for  $C$  ( $\lesssim 0.1$ ) is further supported by the relationship between folding times and  $\sigma$  for several proteins (D.K. and D.T., unpublished).

It can be seen from Table II that there is a good correlation between  $\Omega_c$  and  $\Delta G_{H_2O}$ , which is the free energy difference between the *unfolded state* and the native state. The value of  $\Delta G_{H_2O}$  is normally obtained by extrapolating to zero denaturant concentration which involves errors. More importantly, this analysis of correlation between  $\Omega_c$  and  $\Delta G_{H_2O}$  cannot be carried out easily in the case of thermal unfolding. As a result it appears that it is more convenient to analyze cooperativity data in terms of  $\sigma$ , which can be estimated using our empirical criterion for both thermal and chemical unfolding transitions.

By comparing the range of  $\sigma$  values for two and three state folders (see Tables I, II, III) we can conclude that proteins with  $\sigma \lesssim 0.25$  should exhibit an all-or-none transition. If  $\sigma \gtrsim 0.25$ , then one should anticipate a three (or more) state folding transition. The value of  $\sigma \sim 0.25$ , at which crossover from two state behavior to a three state transition takes place, should be viewed as a rough estimate.

#### IV. CONCLUSION

One of the most important characteristics of protein folding is that the equilibrium folding transition is cooperative [9]. The minimal models (lattice and off-lattice) without side chains capture this cooperativity only in a qualitative manner [1–6]. If a quantitative description of this process is required, then, as demonstrated here and elsewhere [8], a coarse grained description of side chains becomes necessary. Inclusion of side chains into a lattice model of even a small sized chains gives enhanced cooperativity. In these more realistic models cooperativity is due to the possibility of denser packing [16] of the interior of the folded protein. It is clear from the results for  $N = 27$  without side chains that the degree of cooperativity approaching that seen in two state folding of real proteins can be easily achieved by including side chains.

We have shown that there is a correlation between the measure of cooperativity  $\Omega_c$  (see Eq. (11)) and  $\sigma = (T_\theta - T_f)/T_\theta$ . Sequences with small  $\sigma$  fold in a two state manner with large values of  $\Omega_c$ . This is the case for lattice models as well as real proteins. The estimates of  $\sigma$  for two state folders were made using the parameterization of experimental data, measuring the fraction of the native state. Since there are two transitions involved it would be desirable to obtain  $T_\theta$  using entirely different probe (for example, by measuring the radius of gyration). Such measurements would be required to firmly establish the relationship between  $\Omega_c$  and  $\sigma$ . In the absence of such measurements our estimate of  $\sigma$  for two state folders based on Eq. (16) is expected to be only approximate.

Proteins, which require a three state model to describe their folding transition, are expected to have relatively large  $\sigma$ . Based on this classification, we expect that for these proteins the actual cooperative transition should occur from an equilibrium intermediate to the native state as the temperature or denaturant concentration is altered. Such a cooperative transition has in fact been recently reported in the folding of apobovine  $\alpha$ -lactalbumin [38]. The small values of  $\Omega_c$  for the overall  $\mathbf{U} \rightleftharpoons \mathbf{N}$  transition (presumably, resulting from large values of  $\sigma$ ) for lysozyme and apoMb is a reflection of a poor cooperativity of the transition from a random coil to the native state due to the presence of the equilibrium intermediates. This is consistent with a small values of  $\Omega_c$  for transitions  $\mathbf{U} \rightleftharpoons \mathbf{I}$ , while transitions  $\mathbf{I} \rightleftharpoons \mathbf{N}$  are highly cooperative.

The detailed study of the transition to the native state from unfolded conformations in lattice models with side chains suggests a clear mechanism for folding of small proteins that exhibit all-or-none transitions. At a relatively high temperature the backbone becomes "frozen" adopting a native conformation, but side chains are still mobile. Only at lower temperature the side chains become predominantly fixed. The temperature interval, over which this happens, is small for sequences with small  $\sigma$ , so that these sequences are expected to fold kinetically and thermodynamically in a two state manner. This implies that for these sequences pathways should exist, in which the acquisition of the native conformation (backbone and side chains) and the collapse process should be almost simultaneous. Recent molecular dynamics simulations on small peptides also support this notion [39]. It is clear that the enhanced degree of cooperativity in LMSC over LM is due to packing of side chains. A corollary of this result is that denaturation in proteins is basically caused by the disruption of the densely packed side chains as was suggested some years ago by Shakhnovich and Finkelstein [40].

Sequences with moderate or large  $\sigma$  have large difference between the temperatures at which the backbone and side chains adopt native-like conformations. As a result these sequences get trapped in an intermediate, which inevitably slows down the folding kinetics. Explicit kinetic simulations of models with side chains confirm these assertions (D.K. and D.T., unpublished).

## ACKNOWLEDGMENTS

We would like to thank Prof. R. Ulbrich-Hofmann for providing the thermal unfolding data for RNase A in tabular form. We are grateful to W.A.Eaton for suggesting Eq. (17) as a generalization of Eq. (12). We thank J.D.Bryngelson for pointing out reference [36] and T.R. Sosnick for useful discussions. We are also grateful to the referees for penetrating comments. This work was supported in part by a grant from the National Science Foundation (through grant number CHE96-29845).

## REFERENCES

- [1] Dill, K.A., Bromberg, S., Yue, K., Fiebig, K.M., Yee, D.P., Thomas, P.D. & Chan, H.S. (1995). Principles of protein folding - A perspective from simple exact models. *Protein Sci.* **4**, 561-602.
- [2] Bryngelson, J.D., Onuchic, J.N., Socci, N.D. & Wolynes, P.G. (1995). Funnels, pathways and the energy landscape of protein folding: A synthesis. *Proteins Struct. Funct. Genet.* **21**, 167-195.
- [3] Wolynes, P.G., Onuchic, J.N. & Thirumalai, D. (1995). Navigating the folding routes. *Science* **267**, 1619-1620.
- [4] Thirumalai, D., Klimov, D.K., & Woodson, S.A. (1997). Kinetic partitioning mechanisms a unifying theme in the folding of biomolecules. *Theor. Chem. Acct.* **1**, 23-30.
- [5] Dill, K.A. & Chan, H.S. (1997). From Levinthal to pathways to funnels (1997). *Natur. Struct. Biol.* **4**, 10-19.
- [6] Mirny, L.A., Abkevich, V. & Shakhnovich, E.I. (1996). Universality and diversity of the protein folding scenarios: a comprehensive analysis with the aid of a lattice model. *Folding & Design* **1**, 103-116.
- [7] Onuchic, J.N., Wolynes, P.G., Luthey-Schulten, Z.A. & Socci, N.D. (1995). Toward an outline of the topography of a realistic protein-folding funnel. *Proc. Natl. Acad. Sci. USA* **92**, 3626-3630.
- [8] Kolinski, A., Galazka, W., & Skolnick, J. (1996) On the origin of the cooperativity of protein folding: Implications from model simulations. *Proteins Struct. Funct. Genet.* **26**, 271-287.
- [9] Anfinsen, C.B. & Scheraga, H.A. (1975) Experimental and theoretical aspects of protein folding. *Adv. Prot. Chem.* **29**, 205-300.
- [10] Camacho, C.J. & Thirumalai, D. (1993). Kinetics and thermodynamics of folding in model proteins. *Proc. Natl. Acad. Sci. USA* **90**, 6369-6372.
- [11] Fukugita, M., Lancaster, D. & Mitchard, M.G. (1993) Kinematics and thermodynamics of a folding heteropolymer. *Proc. Natl. Acad. Sci.* **90**, 6365-6368.
- [12] Guo, Z., Brooks III, C.L. & Boczko, E.M. (1997) Exploring the folding free energy surface of a three-helix bundle protein. *Proc. Natl. Acad. Sci.* **94**, 10161-10166.
- [13] Zhou, Y. & Karplus, M. (1997) Folding thermodynamics of a model three-helix-bundle protein. *Proc. Natl. Acad. Sci.* **94**, 14429-14432.
- [14] Hao, M.-H. & Scheraga, H. A. (1994) Monte Carlo simulations of a first order transition for protein folding. *J. Phys. Chem.* **98**, 4940-4948.
- [15] Hao, M.-H. & Scheraga, H. A. (1994) Statistical thermodynamics of protein folding: Sequence dependence. *J. Phys. Chem.* **98**, 9882-9893.
- [16] Richards, F. M. (1977) Areas, volumes, packing and protein structure. *Ann. Rev. Bio-phys. Bioeng.* **6**, 151-176.
- [17] Richards, F. M. & Lim, W. (1993) An analysis of packing in the protein folding problem. *Q. Rev. Biophys.* **26**, 423-498.
- [18] Bromberg, S. & Dill, K.A. (1994) Side-chain entropy and packing in proteins. *Protein Sci.* **3**, 997-1009.
- [19] Kolinski, A., Godzik, A., & Skolnick, J. (1993) A general method for the prediction of the three dimensional structure and folding pathway of globular proteins: Application to designed helical proteins. *J. Chem. Phys.* **98**, 7420-7433.



- [20] Miyazawa, S. & Jernigan, R.L. Estimation of effective inter-residue contact energies from protein crystal structures: quasi-chemical approximation. (1985) *Macromolecules* **18**, 534-552.
- [21] Miyazawa, S. & Jernigan, R.L. Residue-residue potentials with a favorable contact pair term and an unfavorable high packing density term, for simulation and threading. (1996) *J. Mol. Biol.* **256**, 623-644.
- [22] Klimov, D.K. & Thirumalai, D. (1996). Factors governing the foldability of proteins. *Proteins Struct. Funct. Genet.* **26**, 411-441.
- [23] Bowie, J.U., Luthy, R., & Eisenberg, D. (1991). A method to identify protein sequences that fold into a known three-dimensional structure. *Science* **253**, 164-170.
- [24] Shakhnovich, E. & Gutin, A.M. (1993). A new approach to the design of stable proteins. *Protein Eng.* **6**, 793-800.
- [25] Shakhnovich, E. (1994). Proteins with selected sequences fold into unique native conformation. *Phys. Rev. Lett.* **72**, 3907-3910.
- [26] Veitshans, T., Klimov, D.K., and Thirumalai, D. (1996). Protein folding kinetics: Time scales, pathways, and energy landscapes in terms of sequence dependent properties. *Folding & Design* **2**, 1-22.
- [27] Ferrenberg, A.M. & Swendsen, R. H. (1989). Optimized Monte Carlo data analysis. *Phys. Rev. Lett.* **63**, 1195-1198.
- [28] Klimov, D.K. & Thirumalai, D. (1996). A criterion that determines the foldability of proteins. *Phys. Rev. Lett.* **76**, 4070-4073.
- [29] Jackson, S.E. & Fersht, A.R. (1991). Folding of chymotrypsin inhibitor 2: 1. Evidence for a two-state transition. *Biochem.* **30**, 10428-10435.
- [30] Arnold, U. & Ulbrich-Hofmann, R. (1997). Kinetic and thermodynamic thermal stabilities of ribonuclease A and ribonuclease B. *Biochem.* **36**, 2166-2172.
- [31] Schonbrunner, N., Koller, K.-P. & Kiefhaber, T. (1997) Folding of the disulfide-bonded  $\beta$ -sheet protein tendamistat: Rapid two-state folding without hydrophobic collapse. *J. Mol. Biol.* **268**, 526-538.
- [32] Plaxco, K. W., Spitzfaden, C., Campbell, I. D. & Dobson, C. M. (1997) A comparison of the folding kinetics and thermodynamics of two homologous fibronectin type III modules. *J. Mol. Biol.* **270**, 763-770.
- [33] Sancho, J., Neira, J. L. & Fersht, A. R. (1992) A N-terminal fragment of barnase has residual helical structure similar to that in a refolding intermediate. *J. Mol. Biol.* **224**, 749-758.
- [34] Barrick, D. & Baldwin, R.L. (1993) Three-state analysis of sperm whale apomyoglobin folding. *Biochem.* **32**, 3790-3796.
- [35] Chen, L., Hodgson, K.O. & Doniach, S. (1996). A lysozyme folding intermediate revealed by solution X-ray scattering. *J. Mol. Biol.* **261**, 658-671.
- [36] Sosnick, T.R. & Trewhella, J. (1992) Denaturated states of ribonuclease A have compact dimensions and residual secondary structure. *Biochem.* **31**, 8329-8335.
- [37] Luo, Y., Kay M.S. & Baldwin, R.L. (1997) Cooperativity of folding of the apomyoglobin pH 4 intermediate studied by glycine and proline mutations. *Nature Struct. Biol.* **4**, 925-930.
- [38] Balbach, J., Forge, V, van Nuland, N. A., Winder, S. L., Hore, P. J. & Dobson, C. M. (1995) Following protein folding in real-time using NMR-spectroscopy. *Nature Struct. Biol.*

- Biol.* **2**, 866-870.
- [39] Mohanty, D., Elber, R., Thirumalai, D., Beglov, D. & Roux, B. (1997) Kinetics of Peptide Folding: Computer Simulations of SYPFDV and Peptide Variants in Water *J. Mol. Biol.* **272** , 423-442.
- [40] Shakhnovich, E. I. & Finkelstein, A.V. (1989) Theory of cooperative transitions in protein molecules. I. Why denaturation of globular protein is a first order phase transition. *Biopolym.* **28**, 1667-1680.

## FIGURES

**Fig. 1.** Native conformations and energy spectra of sequences A (upper panel) and B (lower panel). The sequences for A and B are also displayed. The first letter corresponds to residue labeled 1. The energy spectra for the two sequences is given on the right. The spectra for the two sequences are divided into two columns. The left column gives the low energy levels for conformations, in which the backbone (and hence most likely the entire structure) is in a non-native state. The right column corresponds to conformations with the backbone in the native state. Sequence A is highly optimized with  $Z = -17.1$  and  $\delta = 0.50$ , whereas sequence B, while having approximately the same  $Z$  score factor of  $-17.9$ , is not well optimized. This is because one can design a sequence with the *same* composition as sequence B has but with smaller  $Z$ . Consequently, the value of  $\delta = 0.74$  for sequence B is larger, which indicates a higher degree of heterogeneity of this sequence. Sequence A has 10 hydrophobic residues, while B has 8. The figure has been generated using RasMol program (R. Sayle, 1995).

**Fig. 2.** Various thermodynamic functions as a function of temperature for sequence A. Fig. (2a) shows  $\langle \chi \rangle$  (solid line) and  $\langle \chi_{bb} \rangle$  (dashed line) (see Eqs. (2) and (4), respectively). The fluctuations  $\Delta\chi$  (solid line) and  $\Delta\chi_{bb}$  (dashed line) are shown in Fig. (2b). The temperature dependence of the specific heat  $C_v$  (solid line) and the derivative of the radius of gyration with respect to temperature  $d\langle R_g \rangle / dT$  (dashed line) are displayed in Fig. (2c). The value of temperature corresponding to the peak in  $C_v$  is associated with  $T_\theta$ , which clearly coincides with the peak in  $d\langle R_g \rangle / dT$ . This demonstrates that  $T_\theta$  is the usual collapse transition temperature. The probability of being in the NBA  $P_{NBA}$  as a function of temperature is given in Fig. (2d) with the horizontal line marking the level of 0.5. The temperature, at which  $P_{NBA}$  is 0.5, is 0.25, which is almost the same value, at which  $\Delta\chi$  has a maximum. Thus, two methods for computing  $T_f$  are equivalent.

**Fig. 3.** Thermally weighted distribution of states  $(\chi, E)$  calculated for sequence A (upper panel) and sequence B (lower panel). The most populated states  $(\chi, E)$  are shown in red. This figure clearly shows that, at the folding transition temperature  $T_f$ , sequence A samples two distinct thermodynamic states - native basin of attraction and the random coil (unfolded) states. Sequence B, on the other hand, samples at  $T_f$  at least three distinct states with different  $\chi$  and  $E$ . We expect the thermodynamic transition for sequence A to be two state like, whereas sequence B is better described by a three state analysis.

**Fig. 4** Dependence of cooperativity  $\Omega_c$  on  $\sigma_T$  for 3D 15-mer sequences without side chains (full circles) and with side chains (empty circles). Solid line is a guide to eye.

**Fig. 5** Dependence of cooperativity index  $\Omega_c$  on  $\sigma_T$  for 2D 15-mer sequences with side chains and different interaction matrices: random site model (diamonds), MJ shifted potentials (full circles), MJ potentials (empty circles), KGS shifted potentials (triangles), KGS potentials (squares). Shifted MJ or KGS potentials are obtained by setting  $\langle B_0 \rangle = 0$ , where  $\langle B_0 \rangle$  is the interaction energy averaged over all pairs of residues. The values of  $\sigma_T$  and  $\Omega_c$  are obtained by exact enumeration. Solid line is a guide to eye.

**Fig. 6** Dependence of cooperativity index  $\Omega_c$  on  $\sigma_T$  for 3D 27-mer sequences without side chains. The solid line is a guide to eye.

**Fig. 7** Dependence of the collapse temperature  $T'_\theta$  estimated using Eq. (16) on actual collapse temperature  $T_\theta$  determined from the peak of specific heat  $C_v$  for 27-mer LM sequences. The solid line is a guide to eye.

**Fig. 8** Variation of the cooperativity index  $\Omega_c$  on  $\sigma$  for CI2 (thermal unfolding - full circles, chemical unfolding - empty circle), tendamistat (square), and RNase A (triangle),  $^{10}$ FNIII (star), lysozyme (diamond), and apoMb (crosses). We did not show the results for the barnase fragment and  $^9$ FNIII, because  $\Omega_c$  is too small for them. This figure shows that cooperativity can be parameterized by  $\sigma$ , which can be experimentally determined.

TABLES

TABLE I. Temperature Induced Unfolding: Two State Folders

Protein	experimental values		theoretical estimates		
	pH	$T_f, ^\circ C$	$T_\theta, ^\circ C^c$	$\sigma$	$\Omega_c$
CI2 <sup>a</sup>	2.2	41.5	55.5	0.25	5.9
	2.5	47.1	59.8	0.21	9.1
	2.8	55.1	67.5	0.18	13.1
	3.2	63.9	75.2	0.15	21.2
	3.5	70.9	81.5	0.13	29.3
RNase A <sup>b</sup>	8.0	60.3	65.2	0.08	99.4

<sup>a</sup> reported in [29]

<sup>b</sup> reported in [30]

<sup>c</sup> estimated using Eq. (16)

TABLE II. Chemically Induced Unfolding: Two State Folders

Protein	experimental values	theoretical estimates	
	$\Delta G_{H_2O}, kcal\ mol^{-1}$	$\sigma$	$\Omega_c$
Tendamistat <sup>a</sup>	8.13	0.17	13.7
CI2 <sup>b</sup>	7.03	0.20	9.9
<sup>10</sup> FNIII <sup>c</sup>	6.1	0.22	7.5
<sup>9</sup> FNIII <sup>c</sup>	1.2	0.60	0.28
Barnase fragment <sup>d</sup>	1.1	0.62	0.25

<sup>a</sup> GdnHCl induced denaturation reported in [31]

<sup>b</sup> GdnHCl induced denaturation reported in [29]

<sup>c</sup> GdnHCl induced denaturation reported in [32]

<sup>d</sup> Trifluoroethanol induced denaturation reported in [33]

TABLE III. Three State Folders

Protein	pH	C, [Urea]	$\sigma$	$\Omega_c(\mathbf{U} \rightleftharpoons \mathbf{I})$	$\Omega_c(\mathbf{I} \rightleftharpoons \mathbf{N})$
Lysozyme <sup>a</sup>	2.9	–	0.21	–	9.1
ApoMb <sup>b</sup>	–	0.0	0.41	3.4	10.5
	–	1.0	0.34	4.3	19.3
	–	1.5	0.32	3.7	24.7
	–	2.0	0.32	2.7	40.2
ApoMb <sup>c</sup>	4.2	–	–	1.2 <sup>d</sup>	–
	4.2	–	–	5.0 <sup>e</sup>	–

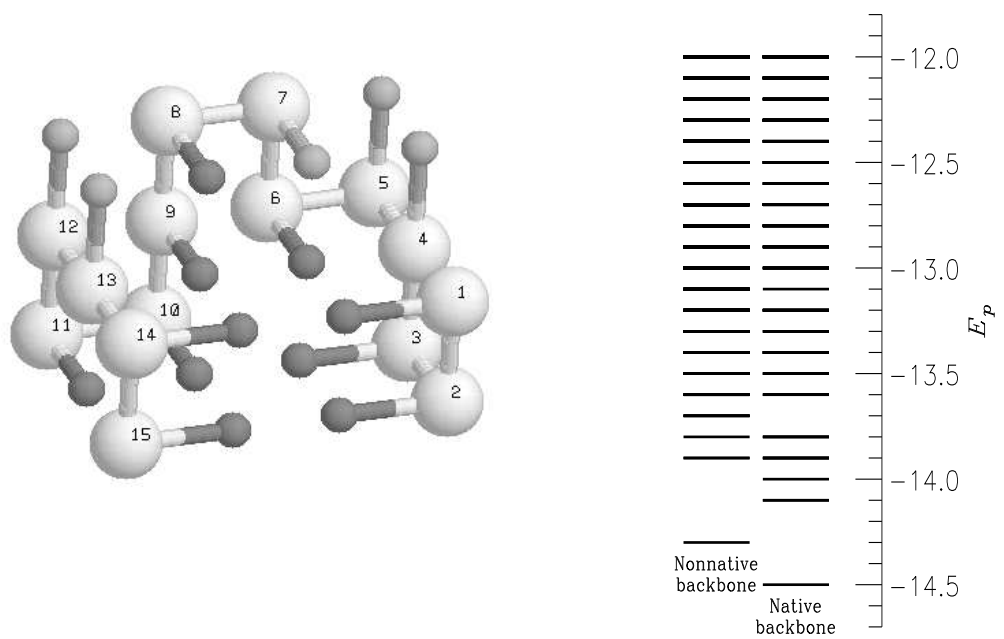
<sup>a</sup> Urea induced denaturation at pH=2.9 and  $T = 20^\circ\text{C}$  monitored by  $R_g$  reported in [35]

<sup>b</sup> pH induced denaturation at  $T = 0^\circ\text{C}$  monitored by CD signal reported in [34]

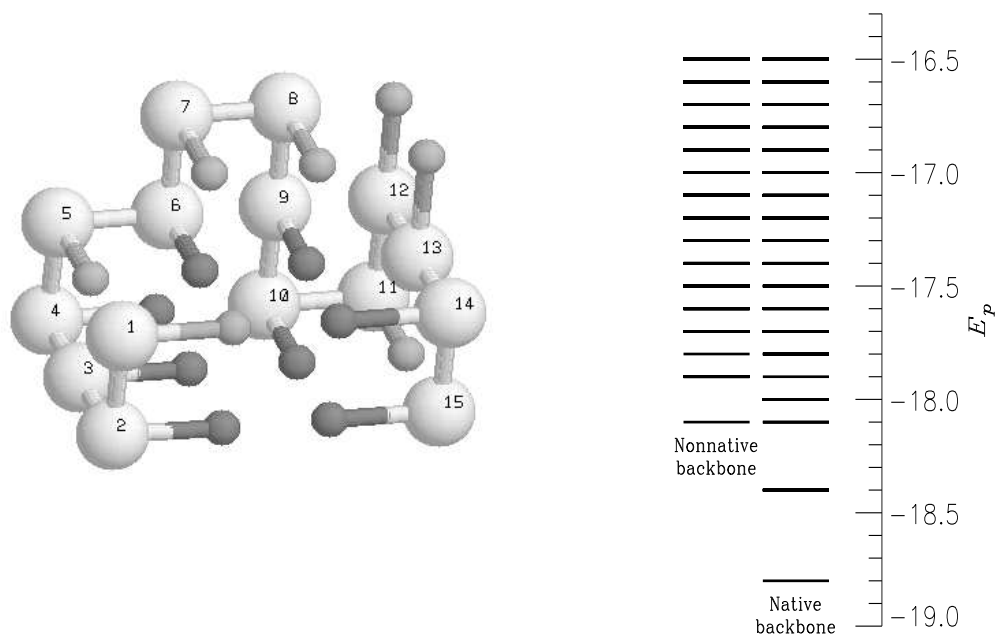
<sup>c</sup> Urea induced transition at pH=4.2 and  $T = 4^\circ\text{C}$  monitored by fluorescence reported in [37]

<sup>d</sup> 20 mM  $\text{Na}_2\text{SO}_4$

<sup>e</sup> 50 mM  $\text{NaClO}_4$



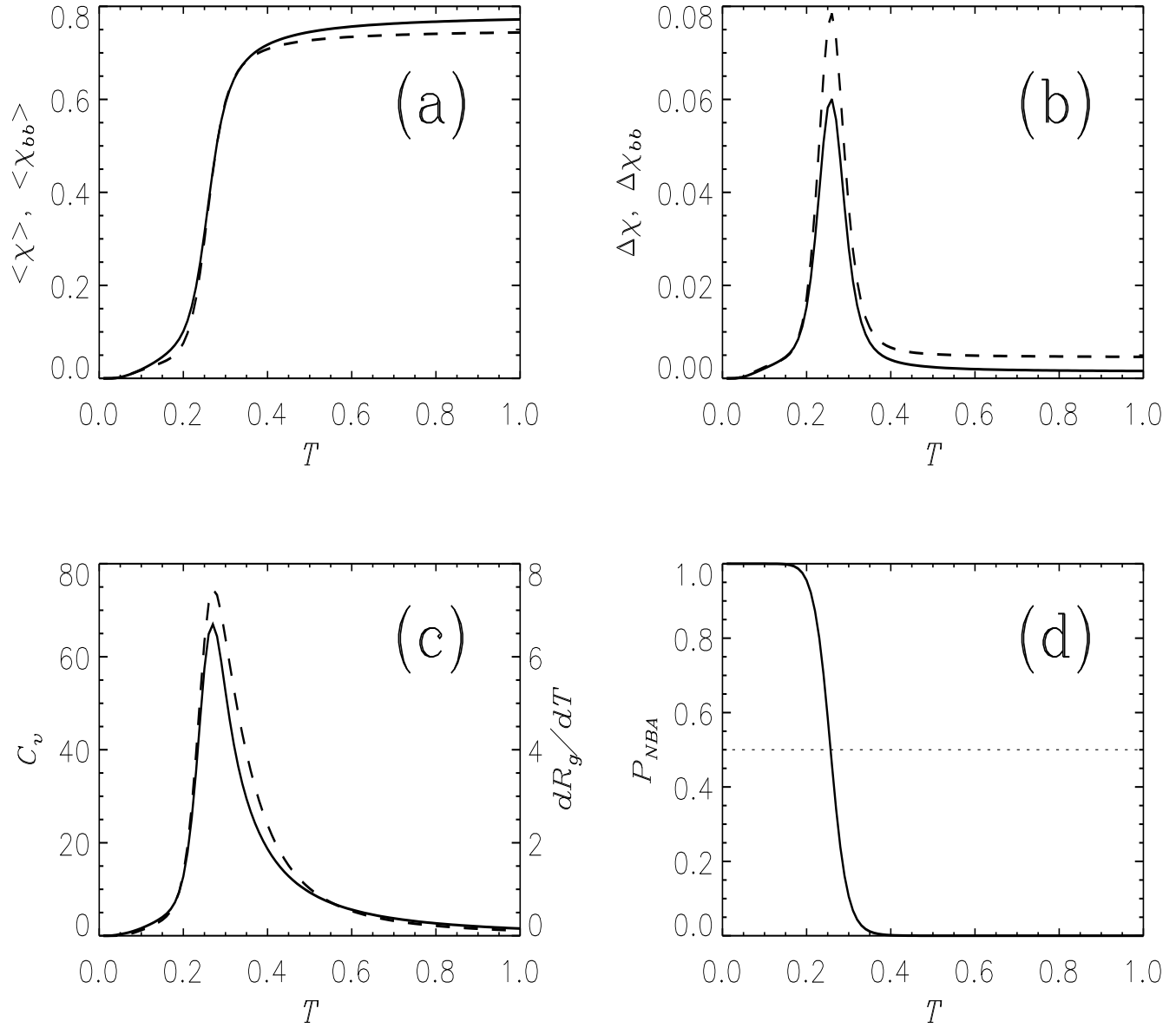
**A:** WVVEKWHYYVANNV



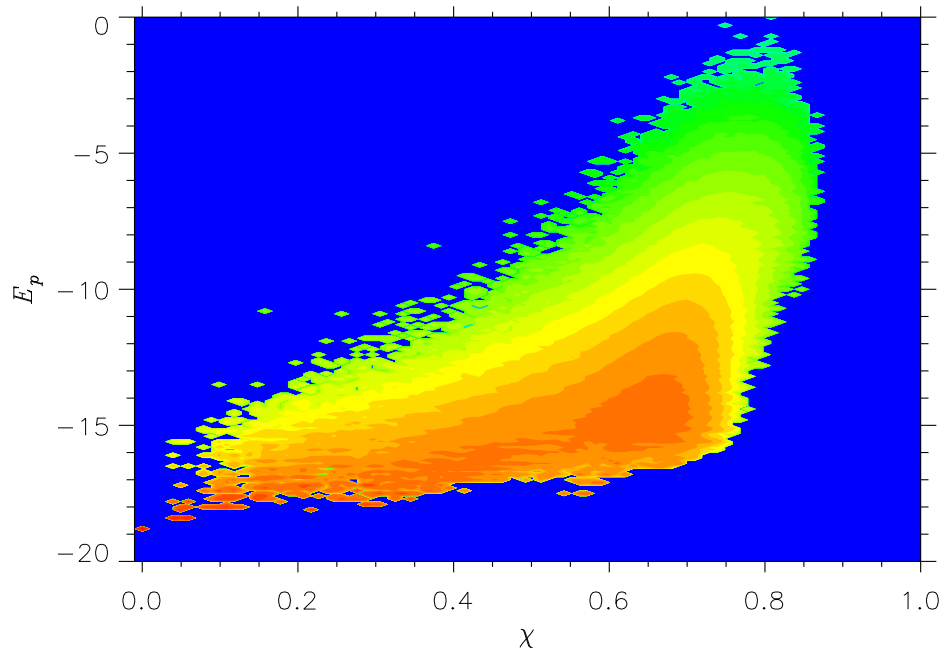
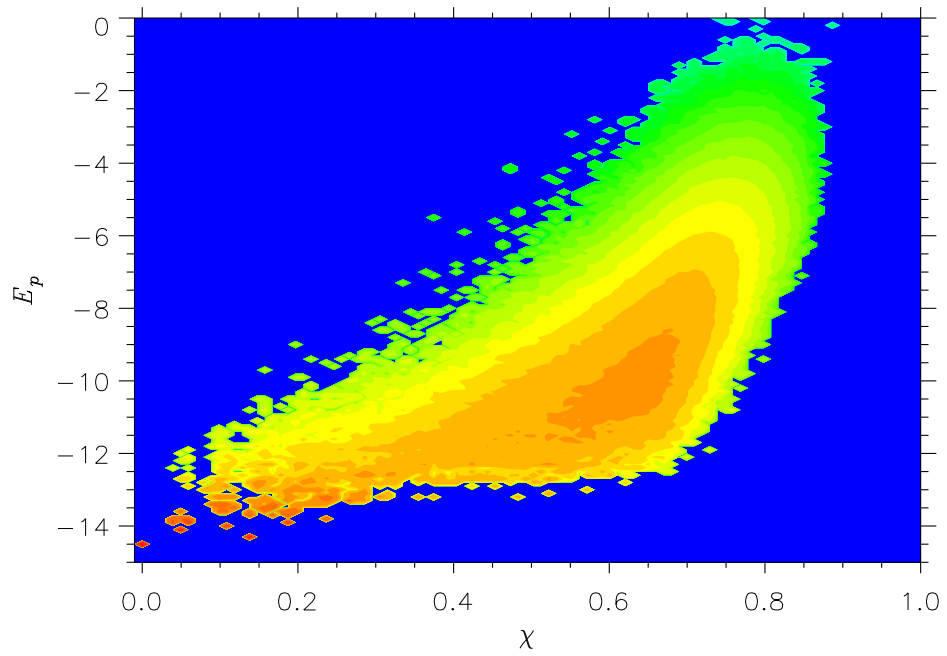
**B:** HCFIYQRWFRKECM

Fig. 1





**Fig. 2**



**Fig. 3**

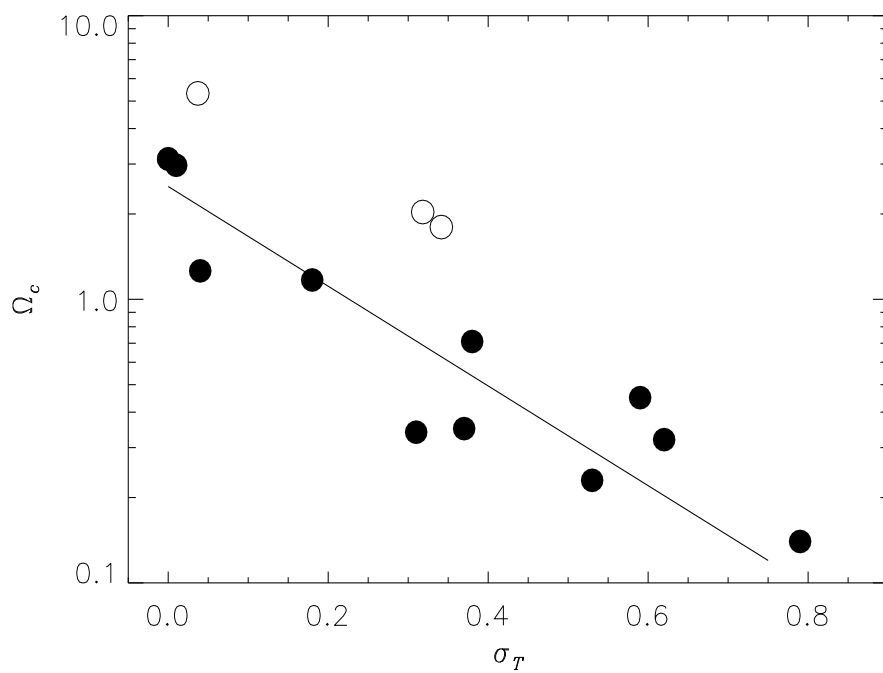


Fig. 4

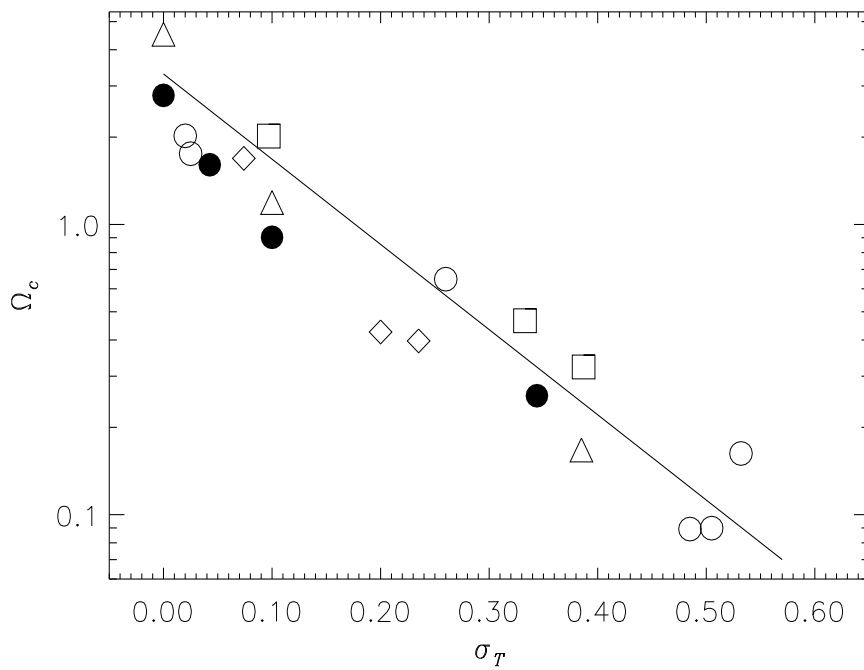
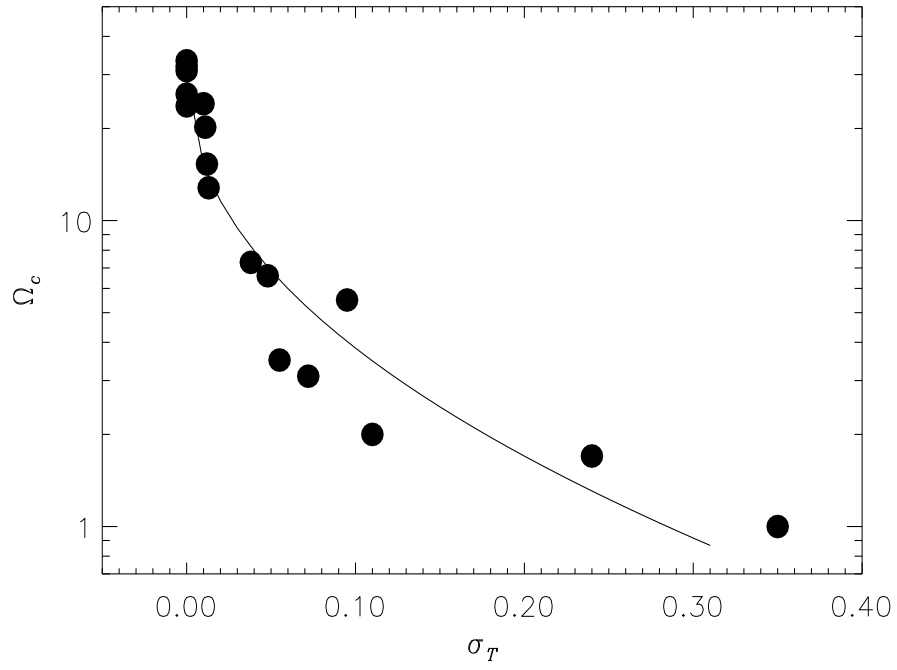
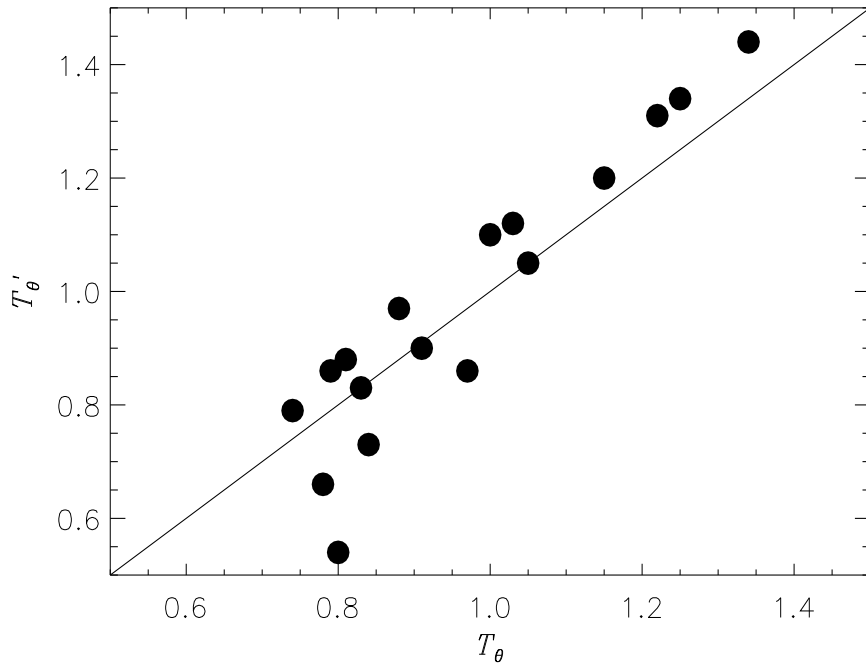


Fig. 5



**Fig. 6**



**Fig. 7**

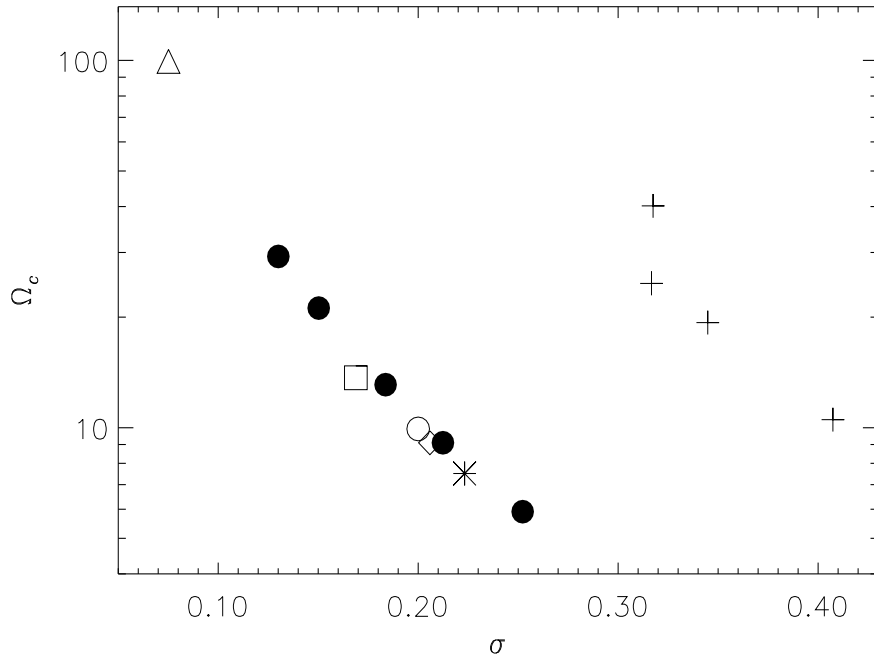


**Fig. 8**